Composite Structures 321 (2023) 117262

Contents lists available at ScienceDirect

Composite Structures

journal homepage: www.elsevier.com/locate/compstruct

Analysis of stress shielding reduction in bone fracture fixation implant using functionally graded materials

M.M. Shahzamanian [a,c], R. Banerjee [a,b], Narendra B. Dahotre [a,b], Arun R. Srinivasa [c], J.N. Reddy [c,*]

[a] Center for Agile and Adaptive Additive Manufacturing, University of North Texas, 3940 N ELM Street, Denton, TX 76207, USA
[b] Department of Materials Science and Engineering, University of North Texas, 3940 N ELM Street, Denton, TX 76207, USA
[c] Department of Mechanical Engineering, Texas A&M University, College Station, TX 77843-3123, USA

ARTICLE INFO

Keywords:
Finite element analysis
Bone implant
Fracture fixation
Functionally graded materials (FGMs)
Stress shielding

ABSTRACT

Bone density reduction occurs when implants are used to arrest fracture propagation. Bones are stress shielded by the implants when enough loads are not placed on the bones. Stress-shielding occurs when stiffness mismatch between the bone and the fracture fixation implant is significant. The aim of this study was to perform an analysis of stress-shielding reduction using functionally graded material (FGM) implants when Young's modulus vary along the length of the implant. In this study, the finite element method (FEM) was used for the simulation of functionally graded implant mounted on a bone. The effect of FGMs on the reduction of stress-shielding imposed on a bone was studied parametrically by conducting simulations of various two-dimensional (2D) and three-dimensional (3D) computational models. First, a low-fidelity 2D model was created where it was observed that the FGMs were capable of reducing the stress-shielding substantially. Then, high-fidelity models such as single-sided with and without screws as well as double-sided FGM implants with different shapes for consideration of partial cracks were simulated. Several simulations were carried out to investigate the minimum required number of layers in an FGM to avoid stress concentration at the FGM layer interfaces. Furthermore, various material gradations in an FGM were tested to present the FGM gradation index that can reduce the stress shielding. Lastly, it was established convincingly through the finite element simulations that FGMs were able to reduce the stress-shielding on a bone with a crack.

1. Introduction

"Wolff's law" states that bone in a healthy person or animal will remodel itself in response to the loads it is placed under [1–5]. It means that a bone must carry an amount of load at any time to stay healthy in the body, and it is harmful if it does not carry any load. However, an implant must be placed on a fractured bone to heal it and does not let the bone carry any load at the fractured zone in the beginning. In this manner, the implant carries the load instead and the other intact parts of the bone beneath the implant are not under significant loads. The bone loses its density because of lack of load it carries, and this phenomenon is called "*stress shielding.*" In other words, the phrase stress shielding refers to the reduction in bone density as a result of removal of typical stress from the bone by an implant [6–10]. Especially, undesirable stress shielding is problematic if stiffness mismatch between the bone and the fracture fixation implant is considerable [6,11–14]. Fig. 1 shows the stress shielded for typical bones that led to density reduction because of implant placement to heal the fracture. Thus, in order to avoid stress shielding in a rather long bone with an existing fracture at its center, it is imperative to design an implant to be stiff enough at the center and not let the bone carry any load, and on the other hand, the implant must have the lowest possible stiffness at the ends to let the bone carry loads. The importance of "*functionally graded materials (FGMs)*" comes into picture in which the material properties vary smoothly and continuously as a desired function of position along certain dimension(s) of the structure from one point to the other [15,16]. In this study, FEM was used to perform a comprehensive analysis of functionally graded (FG) implant placed on a bone to reduce stress shielding. Various models and analyses (i.e., parametric studies to adjust the composition of the FGMs) were performed to understand the main features of this phenomenon in detail.

Many researchers have investigated the behavior of FGMs using FEM. FGMs have also been simulated in finite element (FE) software,

* Corresponding author.
E-mail address: jnreddy@tamu.edu (J.N. Reddy).

https://doi.org/10.1016/j.compstruct.2023.117262
Received 30 March 2023; Received in revised form 2 June 2023; Accepted 13 June 2023
Available online 17 June 2023

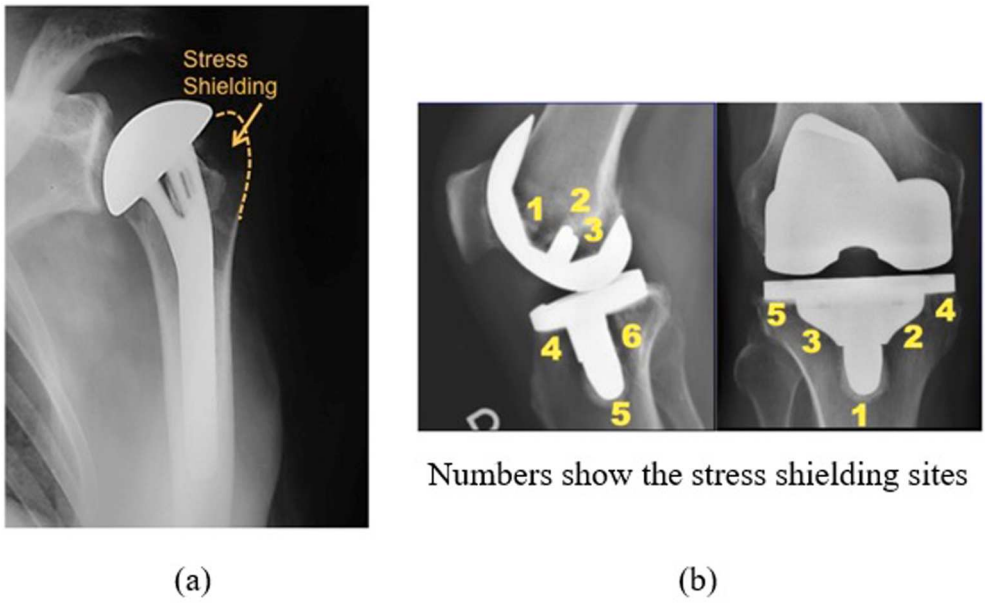

Fig. 1. Stress shielding in bones because of implant placement. (a) Stress-shielded region in a bone close to the shoulder implant [17], and (b) stress-shielded region close to the joints for a knee [18].

such as ANSYS [19] and ABAQUS [20], and various analyses have been performed. In these analyses, the material has been subdivided into several layers in a certain direction, and each layer has a different material property following a gradation relation. For instance, Durodola and Attia [21] simulated FGM and studied the deformation of FG rotating disc under centrifugal loading. FG brake discs have been simulated in ANSYS when material properties vary in radius [22,23] and thickness [24] directions, and thermoelastic contact problems were studied. Ke et al. [25] simulated the FGM and investigated a sliding frictional contact problem. Gunes et al. [26] investigated the elastic–-plastic response of FG circular plates under low impact-velocities using FEM. Gunes et al. [26] investigated the elastic–plastic response of FG circular plates under low impact-velocities using FEM. In their model, the stress–strain curve of layers changed from fully plastic material for a ductile metal to linear elastic material for a brittle ceramic following the intermediate law of mixture.

Not only have FE analyses been performed to investigate the response of FGMs, but also FGMs have been fabricated via various techniques to perform experiments. Both experimental and numerical studies about the effect of elastic–plastic properties variation on low-velocity impact behavior have been performed by Gunes et al. [27]. FGMs have been fabricated using the powder stacking-hot pressing technique experimentally and the Mori–Tanaka scheme has been used to determine the elastic–plastic stress–strain curves of the FGMs layer numerically in Ref. [27]. Moreover, FGMs have been fabricated using the additive manufacturing technique. For instance, in another study, the graded Ti-Nb-Zr alloys with varying compositions have been deposited using double powder feeder arrangement, Ti-35Nb-15Zr (wt %) (in one powder feeder) and pure Ti (in second powder feeder) [28]. The variation in composition has been achieved by varying powder flow rate from both powder feeders during deposition (see Fig. 2). The fabricated FGM contains five layers and the middle layer and the two

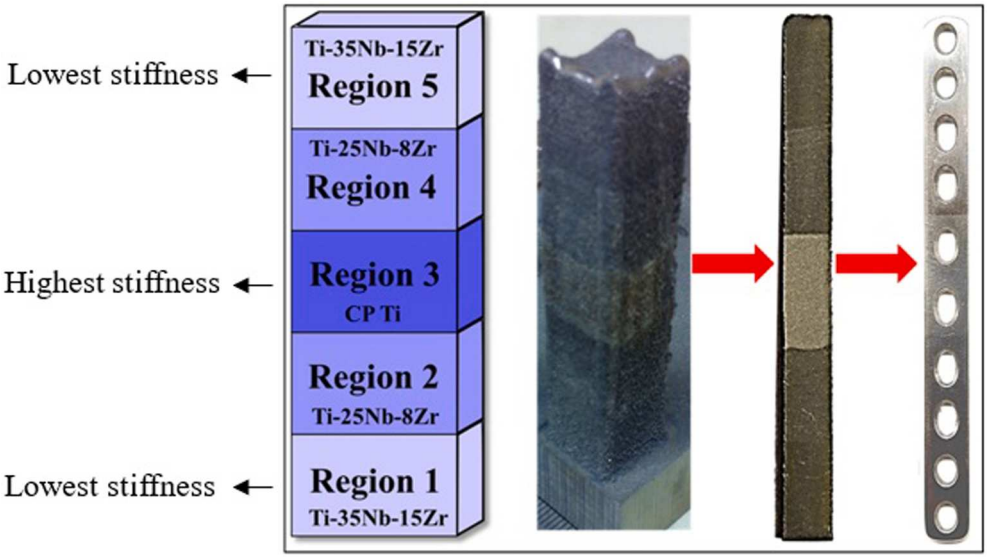

Fig. 2. A FG bar processed via laser engineered net shaping (LENS) by Lima et al [28]. Five layers were fabricated where the middle layer and the end layers have the highest and lowest stiffness, respectively. The oval holes for the installation on bones are shown in the in-plane view of the FG implant.

layers at the ends have the highest and lowest stiffness, respectively. Ti alloys with a high and low contents of "β" stabilizing elements were used to create low and high elastic moduli, respectively. The aim for fabricating such an FGM in [28] was to demonstrate the capability of additive manufacturing technique to fabricate an FGM suitable for biomedical bone implants.

Bone implant for fracture fixation has been designed with various materials [29–31] and different geometries [32–34]. Chandra et al. [35] performed a finite element simulation for bone implant and considered a biodegradable material and observed that the locking compression plate for biodegradable bone implant plate improved the mechanical performances and capabilities. Singh et al. [36] simulated 3D biodegradable implant when the cross-section changed over the length and it was thicker at the center where fracture existed to increase the stiffness of bone implant at the fracture zone. Ganesh et al. [6] simulated a simple model for stiffness graded bone implant under bending and it was concluded that stiffness graded implant reduced the stress shielding. Fice et al. [37] performed a computational study for the tapered fracture fixation plate and it was concluded that such a plate reduced stress shielding because it was stiffer at the center than the other parts of the implant.

In this paper, FGMs were simulated and used as bone implant to investigate their effect on stress shielding. Various models created by FEM were used to scrutinize stress shielding reduction in a bone. Simulation of the FGMs using the ABAQUS commercial finite element software reduces the number of trial-and-error jobs in the fabrication of the functionally graded (FG) bone implant using the additive manufacturing technique. Various effects have been studied and the most suitable and achievable results using an FGM as a bone implant was presented. This approach helps designers understand and investigate to reduce the stress shielding before trying to fabricate an implant on a realistic bone. This article presents an exploratory numerical study to investigate the effect of FGMs on stress shielding reduction in a bone. Therefore, we presented non-dimensionalized results to explain what features must be considered to design and use FGMs as bone implant. Various models were created such as low and high fidelities to understand different effects when other effects were switched off. The main features were investigated one by one and in a stepwise manner to understand how an FGM must be simulated. Lastly, results showed promising approach to use FGM as replacement for bone implant made of pure materials since FGMs were able to reduce the stress shielding.

2. Problem statement and method of solution

Material properties and their variation in the FG plate must be selected in a manner to reduce the stress shielding on the bone. Finite element simulation was used to determine the most suitable material property variations for an FGM. Selection of an appropriate material properties in an FGM implanted on a bone could be selected through running several jobs using finite element commercial software, ABAQUS. Fig. 3 shows the schematic view of the bone with FG implant. The stiffness of the implant must be high at the center of the bone where fracture exists to carry the load and not let the bone carry any load. On the other hand, the stiffness of the implant at the ends must be low enough to let the bone carry loads as much as possible and to reduce the stress shielding.

3. Simulation of FGMs using finite element (FE) software

The material has been subdivided into several layers in a certain direction using commercial finite element software, and each layer had a different material property following a gradation relation [21,22,38]. The schematic view of the low-fidelity model of bone with a mounted FG implant is shown in Fig. 4. Only half of the geometry was simulated due to symmetry. In this schematic, it was assumed that the Young's modulus of the implant at the ends was equal to that of the bone, but such a value could be different in design and analysis.

In this paper, Poisson's ratio was assumed to be constant in an FGM but Young's modulus varied following the Power-law distribution presented in Equation (1) [22]. The layers close to the middle of the bone had the highest Young's modulus value and it decreased along the implant toward the ends. Young's modulus variation along the FG implant changed with material gradation index, m. Fig. 5 shows the Young's modulus variations along the implant for various m values. Young's modulus was nondimensionalized by dividing by the E_{middle} value (Young's modulus at the middle of implant) and the distance over the implant was nondimensionalized by the half length of the implant.

Young's modulus varied linearly when $m = 1.0$. The Young's modulus variation along the length are placed above and below the linear variation ($m = 1.0$) with increasing and decreasing m value, respectively.

$$E = (E_{\text{end}} - E_{\text{middle}}) \times \left(\frac{x}{\frac{L_{implant}}{2}} \right)^{m} + E_{\text{middle}}; 0 \le x \le \frac{L_{implant}}{2} \tag{1}$$

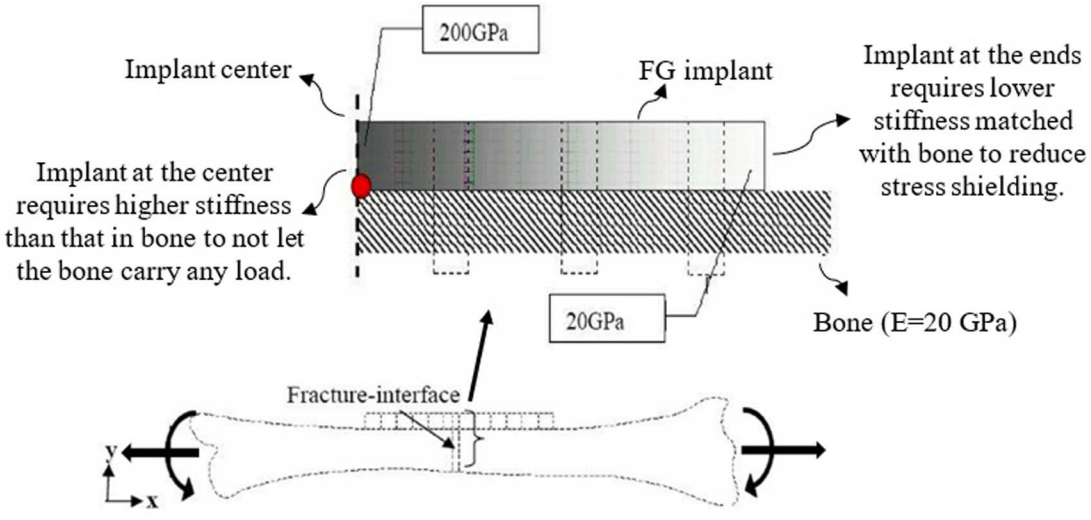

Fig. 3. The importance of FG implant mounted on a bone to reduce the stress shielding. The implant at the middle surface must be stiff to bear the load where fracture at bone occurred, and to place the loads on the bone at the ends to reduce the stress shielding when the FGM at the ends has the lowest possible stiffness [6].

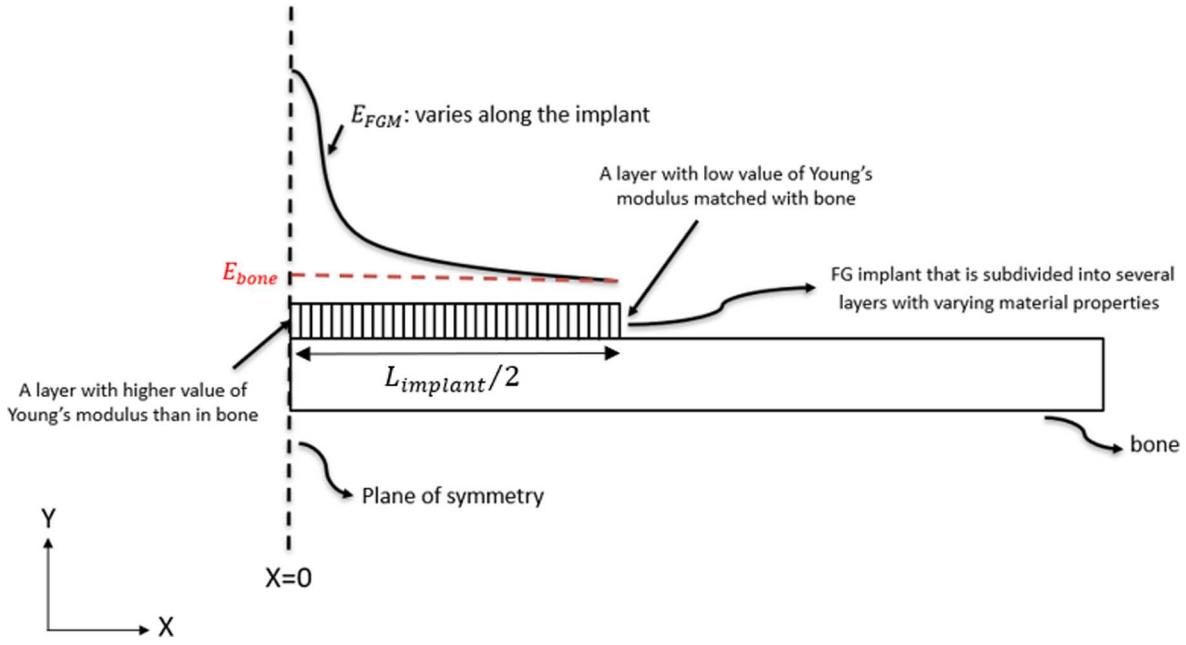

Fig. 4. Schematic of a functionally graded (FG) implant mounted on a bone. Only half of the structure was demonstrated due to the symmetry. Material properties of the FGM varies along the implant. In this schematic, FG implant is tied to the bone, but screws can be used accordingly.

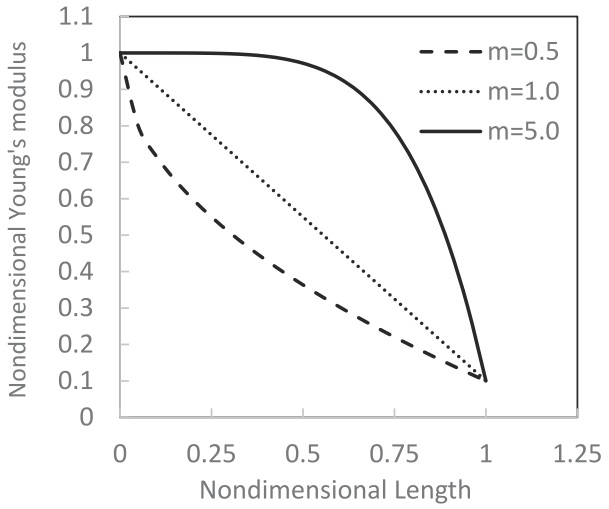

Fig. 5. Young's modulus gradation respect to length with various FGM gradation index following Power-law distribution.

where, m and $L_{implant}$ are gradation index and length of the implant. E is the Young's modulus and subscripts "middle" and "end" reflect the properties at the middle and ends of an implant, respectively.

Python scripts in ABAQUS/Standard was used to simulate the FGMs containing various layers. Every layer had its own material properties, and they were calculated following the Power-law distribution at the centroid of the elements and it was assigned for the whole element. Then, the layers were tied with each other at the interfaces. Finally, the elements were meshed with several elements. A 4-node bilinear plane stress quadrilateral (CPS4) and an 8-node linear brick, (C3D8) were used to simulate the 2D and 3D FGMs, respectively. Fig. 6 shows the simulated typical 3D FG bars with various layers. Every layer in the FGMs could be meshed with coarse or fine elements. The cross-section of the FGMs could be changed to simulate the desired geometry. For instance, the 3D curved cross-sectional FGMs were simulated in this study to be mounted over the bone.

4. Results and discussion

In this section, the finite element results are presented by simulations of two types of low- and high-fidelity models. First, the stress shielding reduction in a bone using a graded stiffness material were tested and investigated with a 2D low-fidelity model. Then, 3D high-fidelity models were simulated to investigate the details of the main features in design to reduce the most stress shielding in a bone. These various models were created to understand the effect of every single parameter and effect individually without existence of the other effects. These details were including the minimum number of layers in an FGM to eliminate the stress concentrations at the interfaces, material gradation index, m, to reduce the most stress shielding. In the high-fidelity model, it was attempted to produce the results without any distortion in a bone because of materials mismatch between the bone and implant. This study mainly aims to investigate the effect of material property gradation on the reduction of stress shielding in a bone implant. Thus, the results and conclusions are not exclusively dependent on the values of the material parameters used in this study. This study only explains how the material gradation in FGMs affect the axial stresses in a bone. Therefore, nondimensional results were presented and the stress values were divided by $E_{\text{middle}} \times \frac{\Delta}{L}$. Where, E_{middle}, Δ, and L are the Young's modulus at the middle of the FG implant, applied displacement at the end of bone, and length of bone, respectively.

4.1. Low-fidelity models: 2D implant with a gap in bones

A 2D low-fidelity model for FG bone implant was simulated to understand the general principals and effects of FGMs on the reduction of stress shielding. As shown in Fig. 7(a), a very simple model was simulated when there was a gap between the two pieces of the bone to consider the existence of fracture. The FGM was consisting of only 5 layers, and it was mounted on one side of the bone and the other side was free. The FGM was tied to the bone in FE simulation. The middle layer of the FGM had the highest Young's modulus value and the Young's modulus decreased to the ends of the implant. The Young's modulus distribution for the FGMs are shown in Fig. 7(a). The Young's modulus of bone was one fifth of the Young's modulus at the FGM in the middle. FGM at the ends had the same stiffness with bone. The deformed

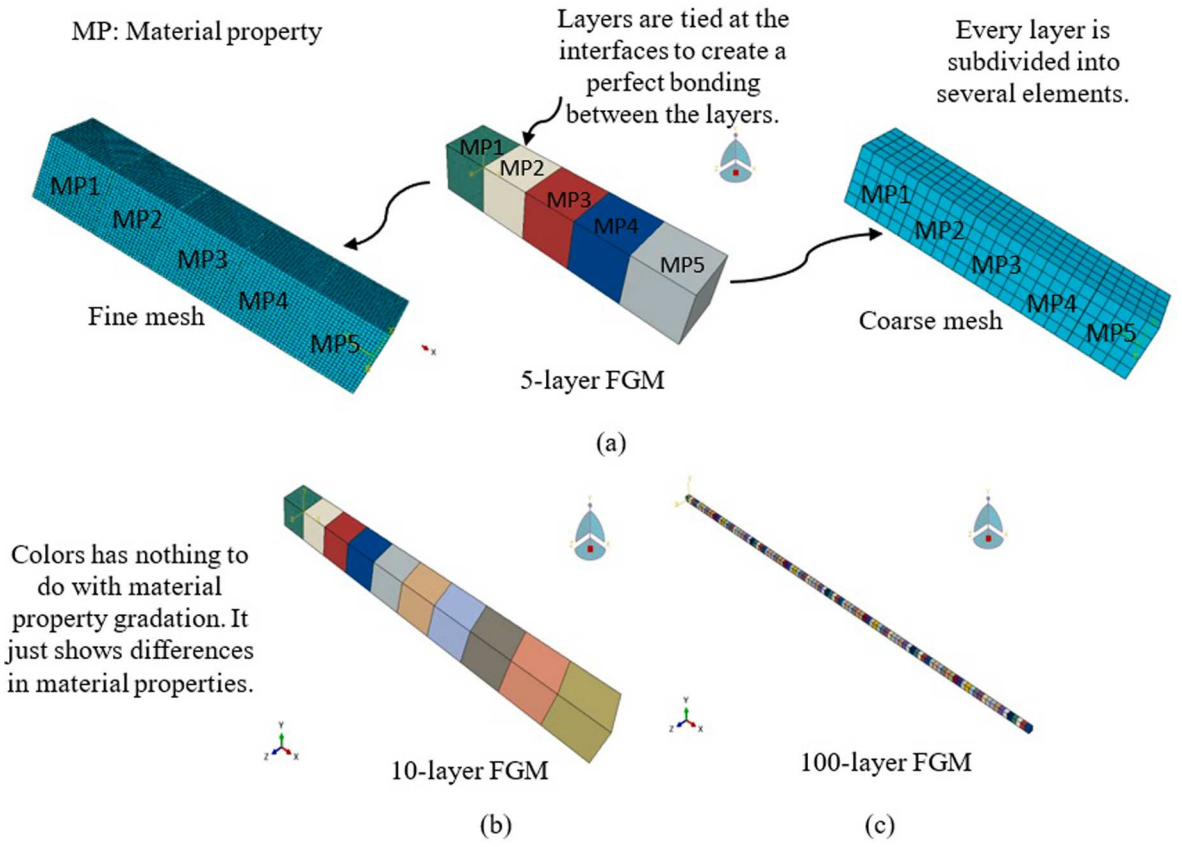

Fig. 6. Simulated FGMs using Python scripts in ABAQUS/standard with various number of layers and material gradation variations. The Python scripts is capable of creating a FG bar containing various number of layers as well as meshing with various element size.

shape of the bone-implant is shown in Fig. 7(b), and it is seen clearly that distortion was unavoidable at the middle where fracture existed. The axial stress imposed on bone and implant are shown in Fig. 7(c) and 7 (d), respectively. The values of axial stress on the bone were compared with those obtained with consideration of a pure material that had the same Young's modulus with the middle layer of the FG implant. Therefore, the axial stress values at the middle were similar for FGM and pure material as shown in Fig. 7(c). It is shown clearly that values of axial stress on bone created with FGM were higher than that with the pure material and this matter showed the reduction of stress shielding using FGMs. The axial stress values on the bone close to the ends of the implant were higher than the other parts of the bone and there was a sharp rising in axial stress. This matter could be justified by the fact that load transferred from the implant to the bone at the implant ends. Fig. 7 (d) shows the axial stress values on the bone and compares the results with FGM and pure material. As expected, the axial stress at the middle of the implant was highest and the axial stress on the implant with pure material was higher than that with FGM. However, at the middle, FGM and pure material had the same Young's modulus but the axial stresses were not the same. The reason was explained because of the created distortion in the bone. Later in this section, it will be seen in Fig. 8 that such a dissimilarity in the axial stress values would be eliminated by avoiding the distortion in a bone using symmetric boundary condition imposed on the free surface of bone.

As observed in Fig. 7(b), distortion was created in the bone under tension. Therefore, symmetric boundary conditions were imposed on the free surface of the bone in the 2D low-fidelity model to eliminate the distortion. Fig. 8(a) shows that the FE configuration for this model. As shown in Fig. 8(b), bone deformed without distortion. The obtained axial stress distributions on bone for FGM and pure material were similar to the cases without imposing symmetric boundary conditions (compare Fig. 7(c) and Fig. 8(c)). However, the axial stress values on implant with FGM and pure material at the center of the implant were similar as shown in Fig. 8(d). This matter exposed the effect of distortion on the distribution of axial stresses on an implant. Furthermore, it is seen in Fig. 7(c) and Fig. 8(c) that the bone material had the lowest value of axial stress at the center where fracture existed, and this matter showed the load bearing capacity of the implant at the center where it was stiffer than the bone material.

4.2. *High-fidelity models: 3D implant with a gap in bones*

Various high-fidelity models including single- and double-sided with and without screws were simulated to understand different parameters for FGM simulations. The finite element results were based on a specific procedure to explain the simulation of FG implant in a step wise manner to understand the main features of stress shielding phenomenon. It was attempted to present the results for the simulation of FGMs in a manner when the finite element results showed the least possible values of distortion in a bone with a conventional implant geometry.

4.2.1. *Single-sided FG implant creates distortion.*

A single-sided FG implant was tested when the Young's modulus varied linearly ($m = 1.0$) following the Power-law distribution. The FG implant contained 20 layers, and the cross-section area were curved in a way to be placed over the bone perfectly. The cross-section of the implant was almost similar to a crescent shape (intersection of two circles). A hollow cylinder was assumed to be a bone. The simulated bone and implant with dimensions are shown in Fig. 9. In order to assume a physical crack at the bone, symmetric boundary condition was only applied at the center of the implant and not to the bone (see Fig. 9). Displacement was applied at the other bone end. As shown in Fig. 9(c),

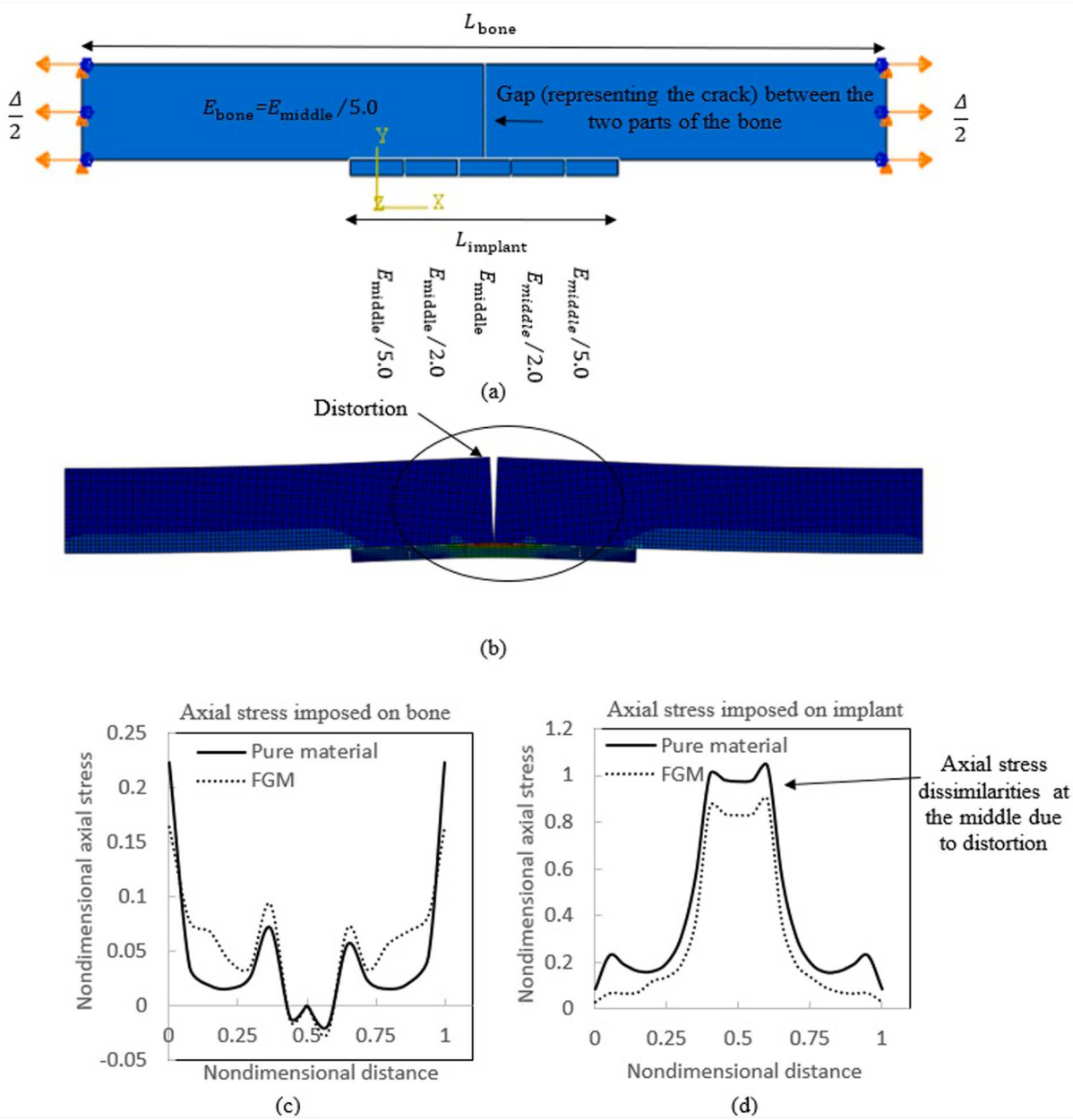

Fig. 7. A 2D single-sided low-fidelity model for FG bone implant to investigate the effect of FGM to reduce the stress shielding without imposing symmetry boundary condition; (a) schematic of FE configuration, (b) deformed shape of the structure under uniaxial tension loads, (c) axial stress distribution on the bone, and (d) axial stress distribution on the implant.

the deformed shape of the bone showed that the single-sided FG implant created distortion at the center where the crack existed there.

4.2.2. Double-sided FG implant eliminates distortion.

In order to eliminate the distortion in bone and to understand the effect of FGM without consideration of distortion, a double-sided FG implant was mounted on a bone. A 20-layer FG implant when the Young's modulus varied linearly ($m = 1.0$) was tested. The simulated bone with implants is shown in Fig. 10. The dimensions and sizes were the same as those simulated for the single-sided FG implant. As it is seen in Fig. 10(c), the distortion was fully eliminated using the double-sided FG implant.

In order to determine the number of layers in an FGM, various FGMs with different number of layers were simulated in a double-sided FG implant on a bone and the effect of every case was studied (Fig. 11(a)). The effect of a 5-layer FGM is shown individually in Fig. 11(b), and it is seen that stress concentration was created at the interfaces of layers in an FGM. The stress concentration decreased with increasing the number of layers for instance in a 10-layer FGM as shown in Fig. 11(c). However, such a stress concentration completely eliminated with consideration of more layers beyond 20 layers in an FGM as shown in Fig. 11(d). In fact, FGMs were subdivided into several layers and the material properties following the gradient variation (Equation (1)) at the centroid of every layer were calculated. If the number of layers is small, the material properties, in this case Young's modulus, of two adjacent layers differ by a significant difference. Therefore, this matter causes a jump on the stress distribution. Consequently, if the number of layers increases, the differences in material properties at the two adjacent layers decreases and it will produce a smooth stress distribution.

Based on the study presented in Fig. 11 to eliminate the stress concentration at the FGM layer interfaces, 20-layer FGM was selected for the further analysis. The effect of material gradation index was investigated

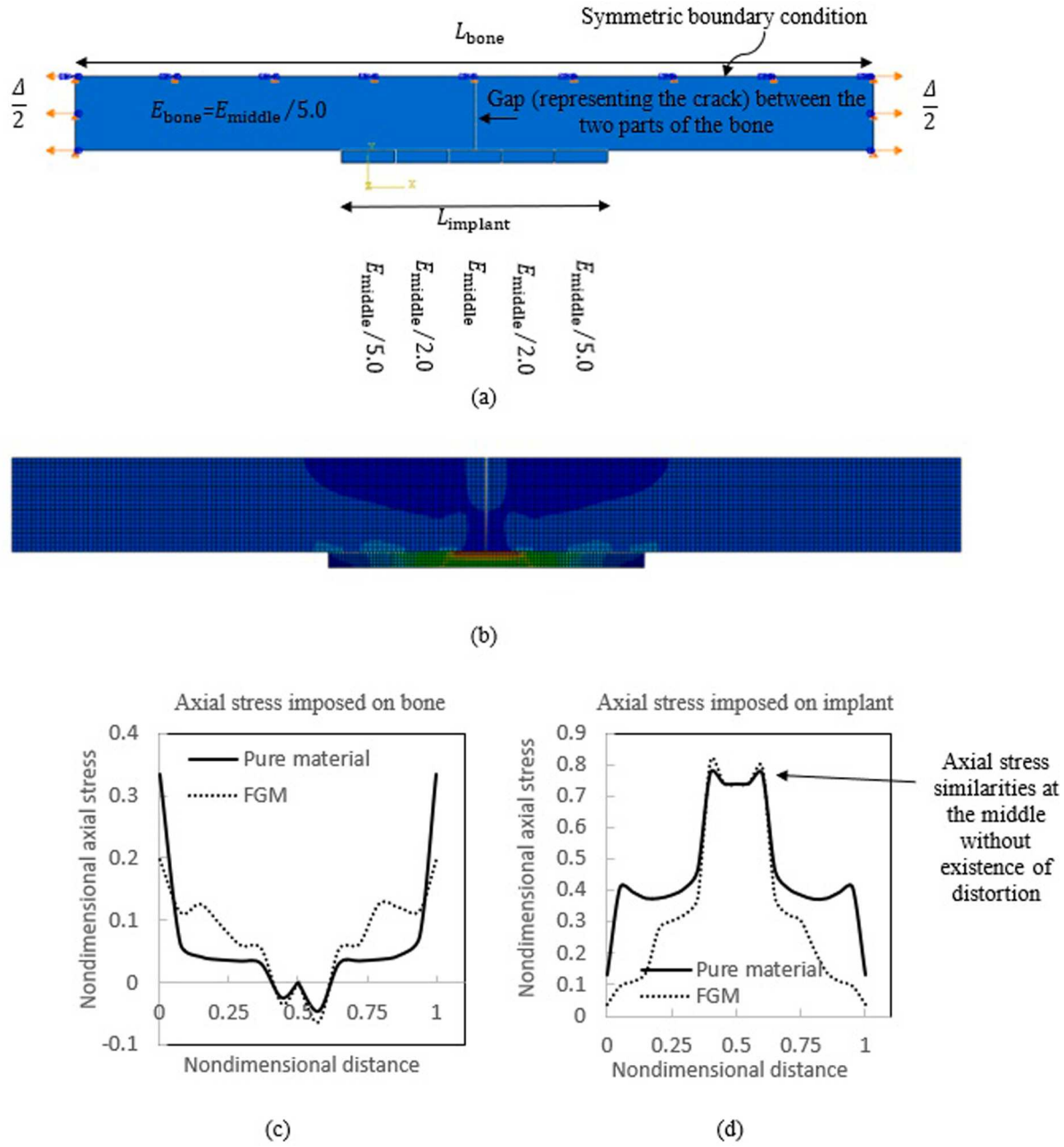

Fig. 8. A 2D single-sided low-fidelity model for FG bone implant with symmetric boundary conditions to avoid distortion at the center of the bone; (a) schematic of FE configuration, (b) deformed shape of the structure under uniaxial tension loads, (c) axial stress distribution on the bone, and (d) axial stress distribution on the implant.

using the double-sided FG implant. The effect of every gradation index was presented and shown in Fig. 12. It is clearly observed that the values of axial stress along the bone increased with decreasing "*m*", and it caused to reduce the stress shielding. The results were compared with those for the pure material that had the same Young's modulus with the layer of the FG implant, and it is seen that the variation of the axial stress was very close to the FGM having $m = 5.0$. Various Young's modulus variation with different values of gradation index are shown in Fig. 5 and it is seen that the properties for the FGM with $m = 5.0$ was close to the pure material particularly at the middle region of the implant.

As mentioned previously, there existed a rising in the axial stress on the bone close to the end of the implant. It was mentioned that such a rising in the axial stress was due the load transfer from implant to the bone. However, such an axial stress rising reached maximum and then started decreasing by moving across the bone. To study the effect of this stress rising, the effect of Young's modulus at the implant ends was investigated when the gradation index was unchanged. For such an investigation, double-sided FGM with 20 layers and $m = 1.0$ was considered. As expected, it was observed that the axial stress value increased along the bone with increasing the Young's modulus at the ends. It can be said that the value of axial stress at the end was high enough for every case to avoid stress shielding. Therefore, it was not required to consider the stress shielding reduction in this region. Even though the low Young's modulus at the implant end had the lowest axial stress, such an Young's modulus reduced the stress shielding in the rest of the bone under implant remarkably. Surfaces of bone which were free and under the bone were marked in Fig. 13. Thus, it was deducted to pick the lowest possible Young's modulus at the implant end. It must be emphasized that these justifications were made based on the results given by ABAQUS.

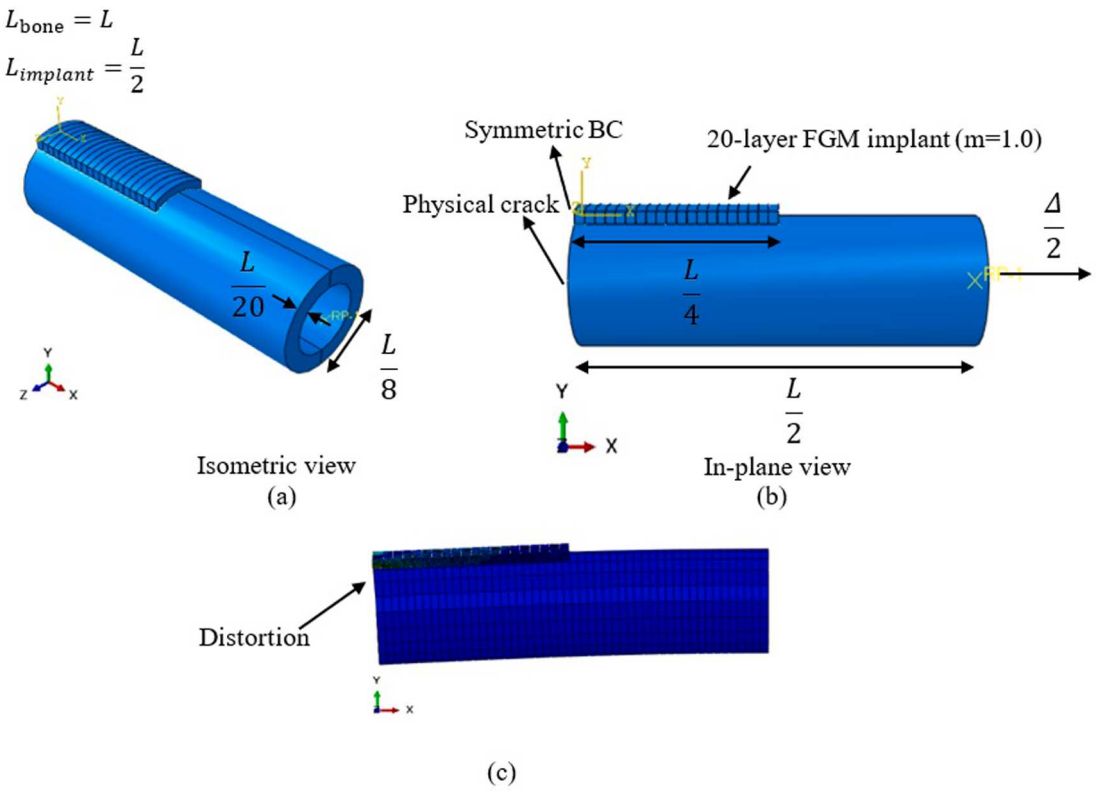

Fig. 9. A single-sided FG implant mounted on a hollow bone with imposed symmetric boundary condition at the center of the implant. A gap existed at the center of bone resembled the fracture.; Geometries are shown in (a) isometric view, and (b) in-plane views. Single sided FG implant created distortion as observed in the deformed shape of bone (c). [only half of the bone with implant is shown due to the symmetry].

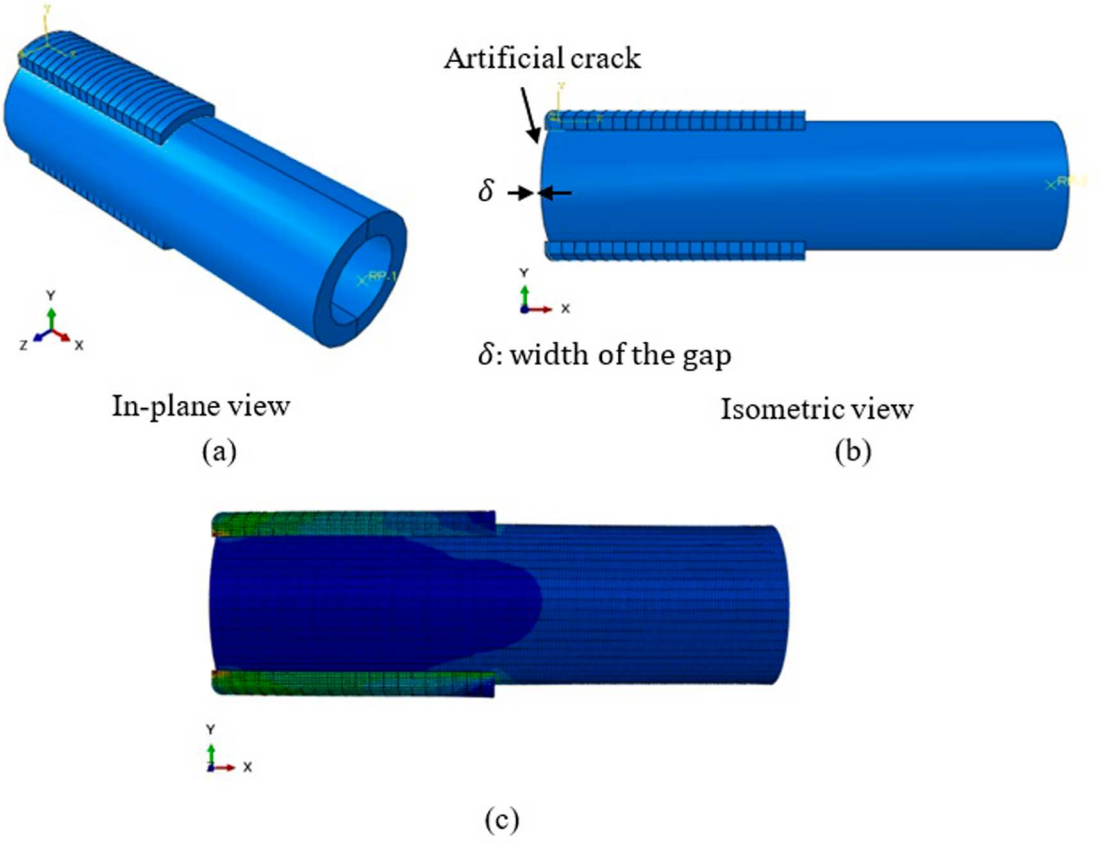

Fig. 10. A double-sided FG implant mounted on a hollow bone with imposed symmetric boundary condition at the center of the two implants. A gap existed at the center of bone resembled the fracture.; Geometries are shown in (a) isometric view, and (b) in-plane views. Double sided FG implant deformed without distortion as observed in the deformed shape of bone (c).

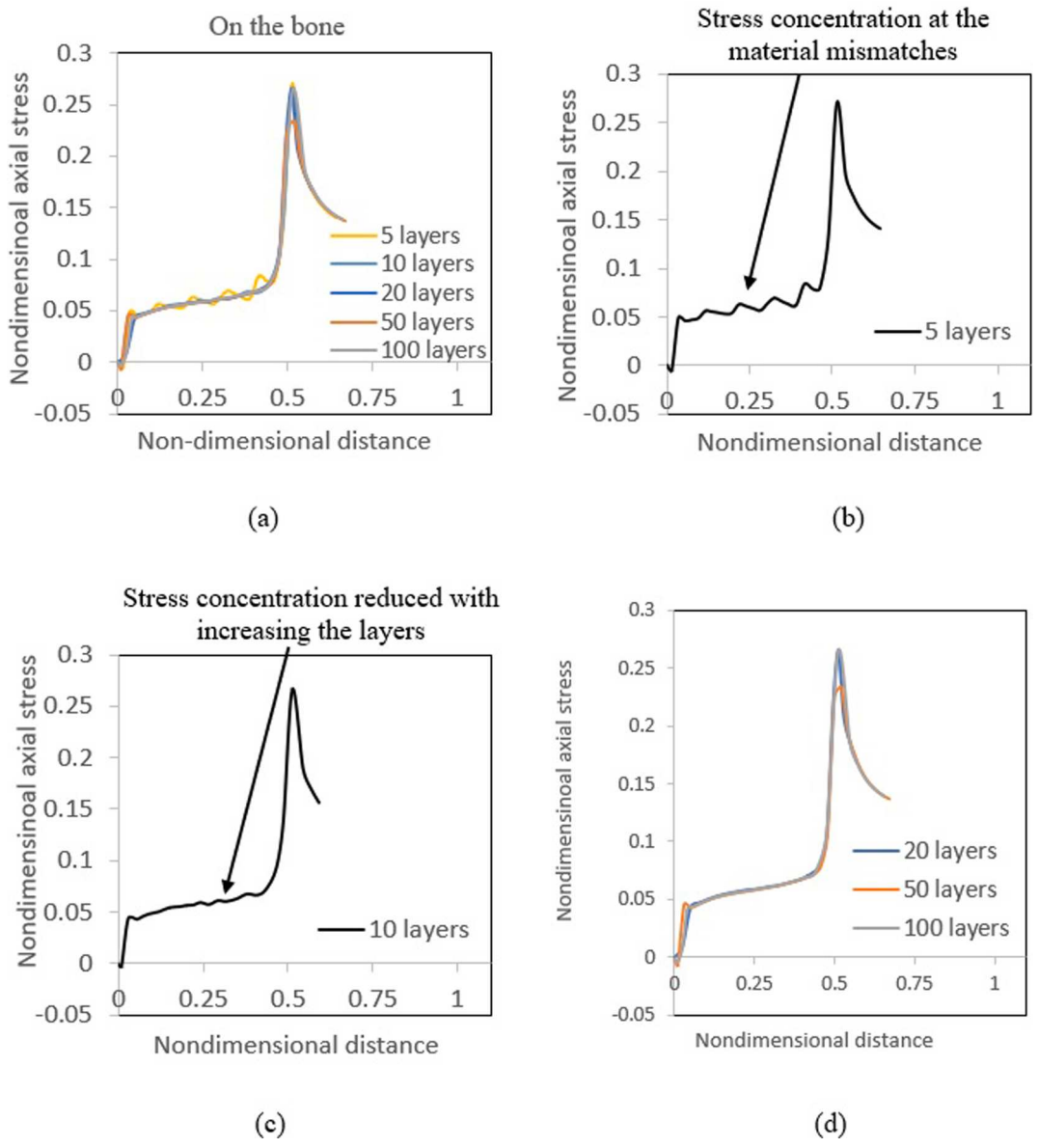

Fig. 11. Effect of number of layers in an FGM on axial stress imposed on a bone. Results show that the stress concentration at the FGM layers decreased or completely eliminated with increasing the number of layers.

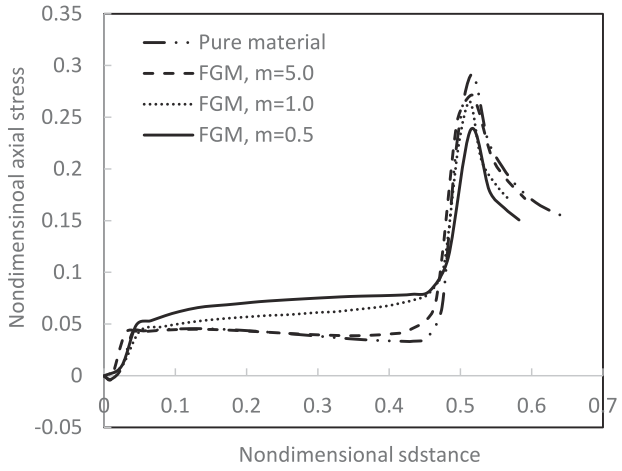

Fig. 12. Effect of material gradation index "*m*" on axial stress imposed on bone. Results show that the stress shielding reduced with decreasing gradation index "*m*".

4.2.3. 3D FG implant with screws

After determination of appropriate number of layers in an FGM as well as material gradation index, *m*, the single-sided FG implant with screws were simulated with various shapes for partial cracks. The simulated bone-implant with screws is shown in Fig. 14 (a-b) and the various shapes for partial crack are shown in Fig. 15. For this simulation, 20-layer FGM with gradation index, m = 0.5, was considered. Five screws were considered to place the FG implant on the bone. A typical geometry for screws was considered since the objective was to study the effect of FGM on reduction of stress shielding in the existence of screws with a typical geometry. In the ABAQUS simulation, screws were tied to the FG implant and bone. Contact constraint between the FG implant and bone surfaces was considered. Fig. 14(c) shows the individual bone with holes, and screws as well as FG implant containing holes.

As shown in Fig. 15, it was assumed that fracture did not occur completely in a bone and instead crack was considered partially. The deformed shape of every case is shown in Fig. 15, and it is observed that distortion occurred only for the bone with a complete crack. Even 25% crack was able to resist distortion in a bone. Fig. 16 shows the vertical

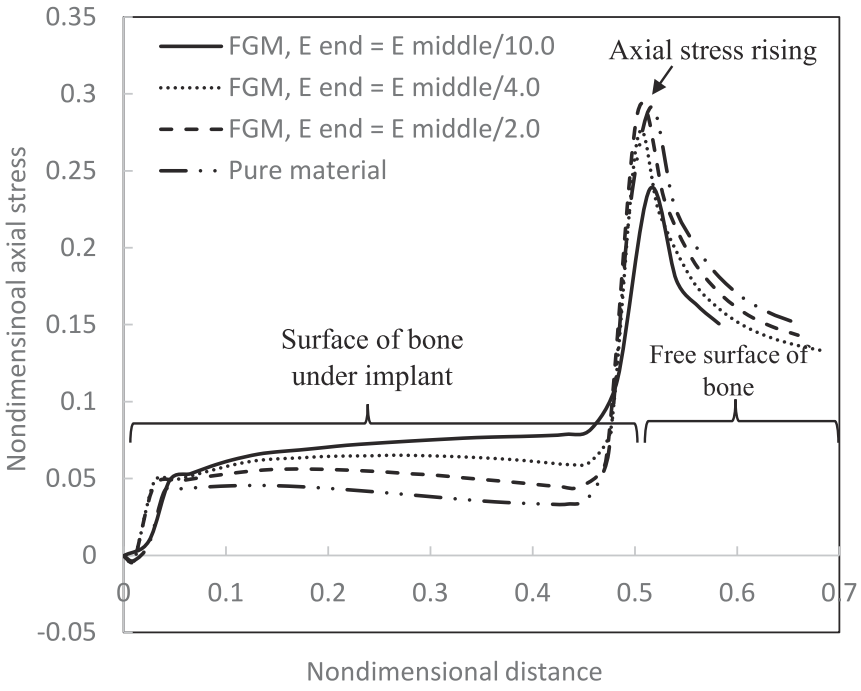

Fig. 13. Effect of Young's modulus at the end of the FG implant on the imposed axial stress on bone. It is observed that there existed a rising in axial stress at the end of the implant where load transferred from bone to the implant.

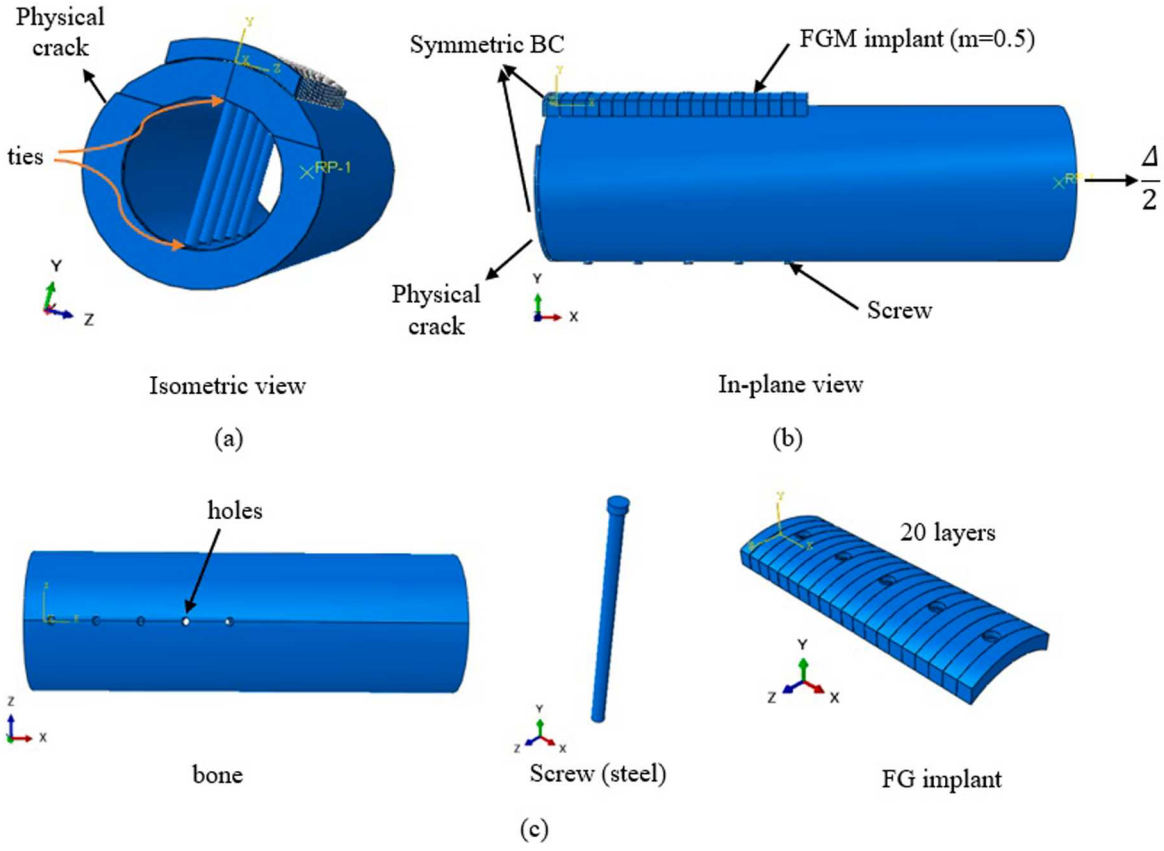

Fig. 14. Single-sided FG implant mounted on a bone with screws. Five screws were used to install the implant and they were tied to the bone and implant accordingly; (a) isometric view, (b) in-plane view, and (c) individual schematic of bone with holes, screw, and FG implant.

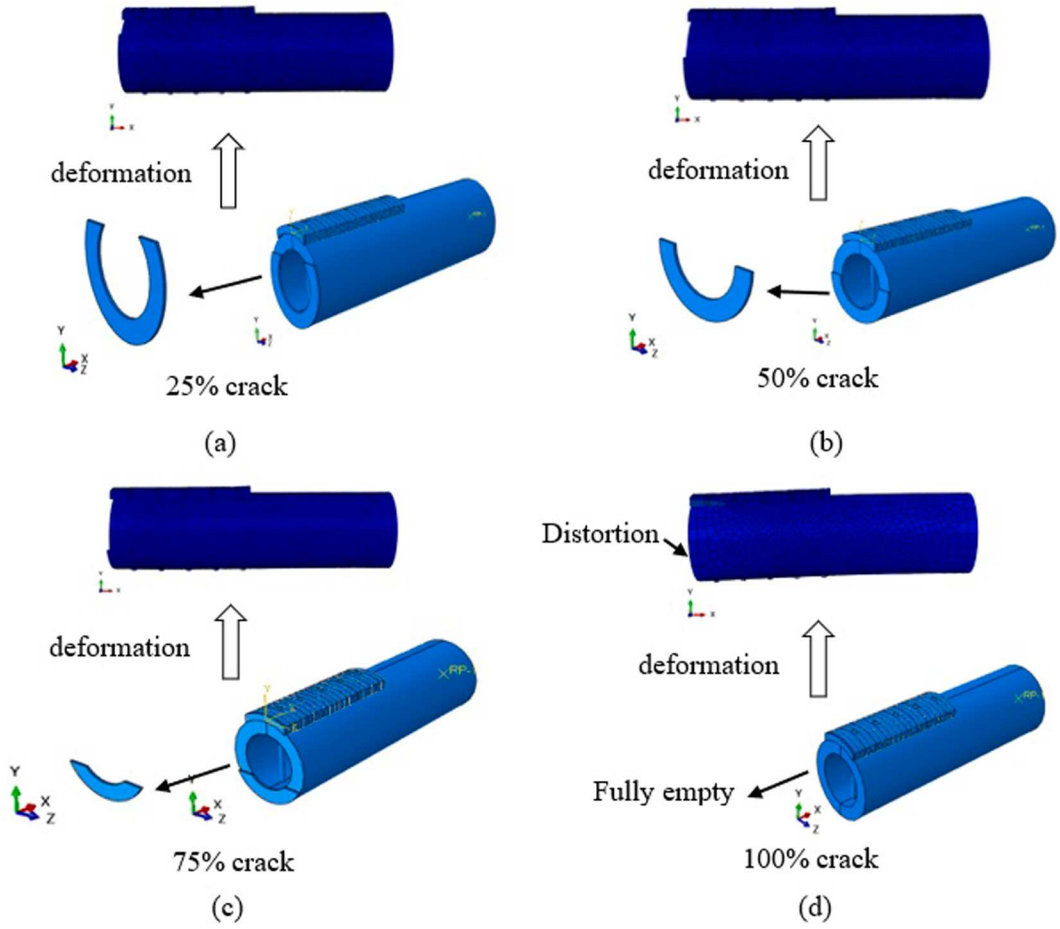

Fig. 15. Various partial crack shapes in a single-sided FG implant mounted on a bone with screws. The deformed shapes of the bone with various crack shapes are presented for every case.

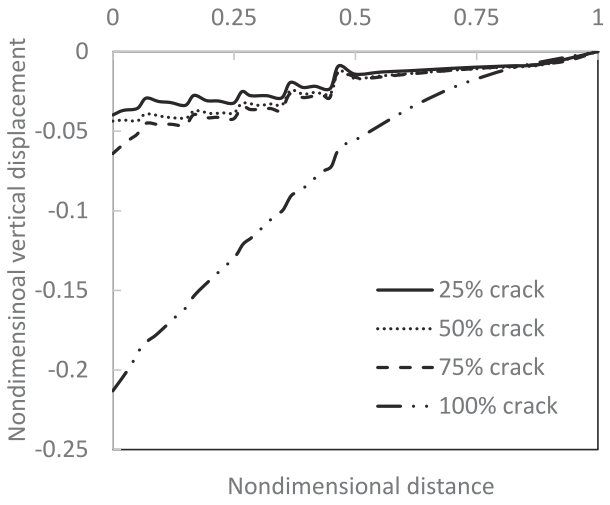

Fig. 16. Nondimensional vertical displacement of the bone versus nondimensional distance over the bone length with single-sided FG implant mounted on bone with screws including various crack shapes.

displacement over the top surface of the bone where the implant was mounted. The vertical displacement and the distance from the middle surface of the bone were nondimensionalized with the outer radius of the bone, and half length of the bone, respectively. It is observed in Fig. 16 that distortion in a bone even with slight partial crack was slight. However, a high value of distortion was observed for fully cracked bone. The main reason to perform such an analysis considering those crack shapes was to get some ideas about eliminating distortion in a bone. However, those crack shapes may not be exactly realistic as happens in a fractured bone. Most importantly, it must be emphasized again that these justifications were made based on the results given by ABAQUS.

Fig. 17 shows the deformed shapes of the bone when an FG implant was mounted on it using five screws. It is observed that the bone was under compression and tension in the regions close to the behind and front of screws, respectively. The axial stress values imposed on bone over length were compared with the case when the pure implant was considered. The results comparison is presented in Fig. 18. Axial stress started decreasing from the symmetry plane to the region right behind the first screw where it was under compression. Then, the axial stress again started decreasing from the region close to the front of the first screw where it was under tension to the region behind the second screw. Fig. 18 shows such a repeated compression-tension axial stress distribution between the holes. It must be emphasized that screws were tied to the bone and FG implant during the simulation and a very slight pressure was placed over the implant and below the bone surface to get the bone/implant surfaces into contact. Results show that such a slight pressure created a remarkable effect of FGM to reduce the stress shielding in a bone more pronouncedly. Results show that the FGM was capable of reducing the stress shielding specially in the regions close to the screws.

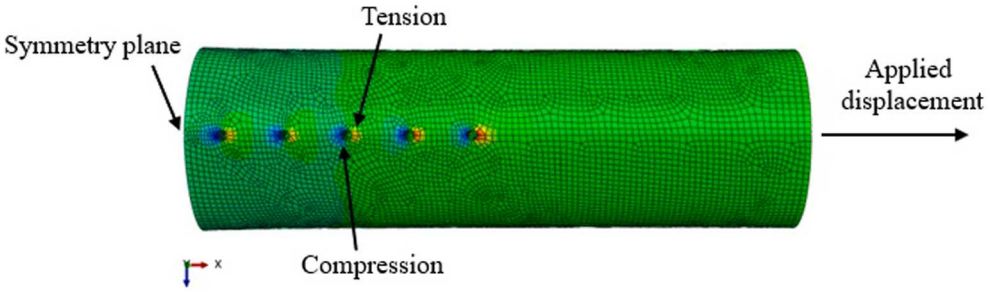

Fig. 17. Deformed shape of the bone when a single-sided FG implant was mounted with screws. Contours blue and red show the compression and tension in the bone, respectively. (For interpretation of the references to colour in this figure legend, the reader is referred to the web version of this article.)

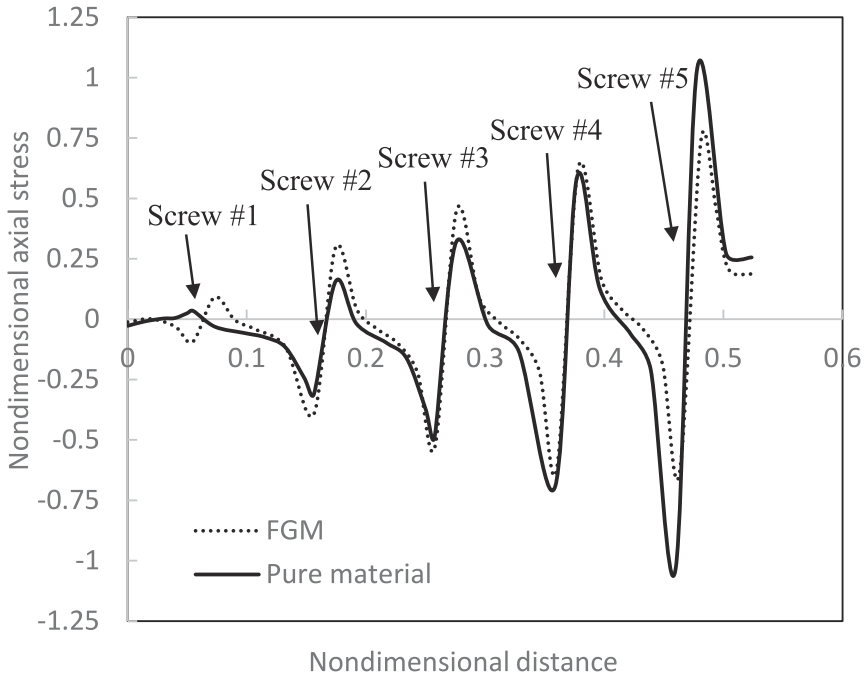

Fig. 18. Axial stress on the bone with FG implant and pure material that had the same Young's modulus with the middle layer of the FG implant.

5. Conclusions

In this study, finite element analyses of bone-implant structure considering FGMs as implant were performed to understand the reduction of stress-shielding in a bone. First, the general principals of the stress-shielding reduction using low-fidelity models were tested. Then, high-fidelity models were simulated to understand the details of the main features of the stress-shielding reduction. The simulations showed that only 20 layers in an FGM was enough to eliminate the stress concentration between the interfaces at the FGM layers. Lower material gradation index than 1.0, in this study $m = 0.5$, following the power-law distribution for Young's modulus over the length reduced the most stress shielding. Finite element results showed that distortion was created in the fully fractured bone using a single-sided implant. However, even a slight partial bone piece at the fracture zone avoided distortion in a bone as predicted by ABAQUS. Otherwise, the simulated results showed that double-sided implant on a bone was required to eliminate the distortion even using screws.

Declaration of Competing Interest

The authors declare that they have no known competing financial interests or personal relationships that could have appeared to influence the work reported in this paper.

Data availability

Data will be made available on request.

Acknowledgement

MMS, RB and NBD acknowledge the infrastructure and support of Center for Agile & Adaptive and Additive Manufacturing (CAAAM) funded through State of Texas Appropriation #190405-105-805008-220 at the University of North Texas. MMS, ARS and JNR would like to acknowledge the partial support of the US National Science Foundation CMMI Grant No. 1952873 in the performance of this work.

References

[1] Chappard D, Baslé M-F, Legrand E, Audran M. Trabecular bone microarchitecture: a review. Morphologie 2008;92(299):162–70.
[2] Gorissen BMC, Wolschrijn CF, van Vilsteren AAM, van Rietbergen B, van Weeren PR. Trabecular bone of precocials at birth; Are they prepared to run for the wolf (f)? J Morphol 2016;277(7):948–56.
[3] Holmes PB, Wolf BJ, Zhou J. A CBCT atlas of buccal cortical bone thickness in interradicular spaces. Angle Orthod 2015;85(6):911–9.
[4] Brodner W, et al. Changes in bone mineral density in the proximal femur after cementless total hip arthroplasty: a five-year longitudinal study. J Bone Joint Surg Brit 2004;86(1):20–6.

[5] Räth C, Baum T, Monetti R, Sidorenko I, Wolf P, Eckstein F, et al. Scaling relations between trabecular bone volume fraction and microstructure at different skeletal sites. Bone 2013;57(2):377–83.
[6] Ganesh V, Ramakrishna K, Ghista DN. Biomechanics of bone-fracture fixation by stiffness-graded plates in comparison with stainless-steel plates. Biomed Eng Online 2005;4(1):1–15.
[7] Niinomi M, Nakai M. Titanium-based biomaterials for preventing stress shielding between implant devices and bone. Int J Biomater 2011;2011:1–10.
[8] Nagels J, Stokdijk M, Rozing PM. Stress shielding and bone resorption in shoulder arthroplasty. J Shoulder Elbow Surg 2003;12(1):35–9.
[9] Sumner DR, Galante JO. Determinants of stress shielding. Clin Orthop Relat Res 1992;274:203–12.
[10] Huiskes R, Weinans H, Van Rietbergen B. The relationship between stress shielding and bone resorption around total hip stems and the effects of flexible materials. Clin Orthop Relat Res 1992:124–34.
[11] Al-Tamimi AA, Peach C, Fernandes PR, Cseke A, Bartolo PJDS. Topology optimization to reduce the stress shielding effect for orthopedic applications. Procedia Cirp 2017;65:202–6.
[12] Arabnejad S, Johnston B, Tanzer M, Pasini D. Fully porous 3D printed titanium femoral stem to reduce stress-shielding following total hip arthroplasty. J Orthop Res 2017;35(8):1774–83.
[13] Torres Y, Trueba P, Pavón J, Montealegre I, Rodríguez-Ortiz JA. Designing, processing and characterisation of titanium cylinders with graded porosity: An alternative to stress-shielding solutions. Mater Des 2014;63:316–24.
[14] Al-Tamimi AA, Fernandes PRA, Peach C, Cooper G, Diver C, Bartolo PJ. Metallic bone fixation implants: a novel design approach for reducing the stress shielding phenomenon. Virtual Phys Prototyping 2017;12(2):141–51.
[15] Suresh S, Mortensen A. Fundamentals of Functionally Graded Materials (The Institute of Materials. London): IOM Communications Ltd.; 1998.
[16] Reddy JN. Analysis of functionally graded plates. Int J Numer Meth Eng 2000;47 (1–3):663–84.
[17] https://www.google.com/search?q=bone+stress+shielding&tbm=isch&ved=2ahUKEwidpKyr3aP5AhXLm2oFHYqLATAQ2-cCegQIABAA&oq=bone+stress+shielding&gs_lcp=CgNpbWcQAzIFCAAQgAQ6BAgjECdQ8QZYxw1gkBJoAHAAeACAAUuIAcYGkgECMTKYAQCgAQGqAQtnd3Mtd2l6LWltZ8ABAQ&sclient=img&ei=LMbmYp3eOMu3qtsPipeGgAM&bih=751&biw=1349&rlz=1C1CHZN_enCA927CA927#imgrc=L1msB6GgSM9rMM.
[18] Bendich I, Lawrie CM, Riegler V, Barrack RL, Nunley RM. The Impact of Component Design and Fixation on Stress Shielding After Modern Total Knee Arthroplasty. J Arthroplasty 2022;37(6). S221-S225.
[19] Thompson MK, Thompson JM. ANSYS mechanical APDL for finite element analysis. Butterworth-Heinemann; 2017.
[20] Abaqus V. 6.14 Documentation. Dassault Systemes Simulia Corporation 2014;651 (6.2).
[21] Durodola J, Attia O. Deformation and stresses in functionally graded rotating disks. Compos Sci Technol 2000;60(7):987–95.
[22] Shahzamanian MM, Sahari BB, Bayat M, Mustapha F, Ismarrubie ZN. Finite element analysis of thermoelastic contact problem in functionally graded axisymmetric brake disks. Compos Struct 2010;92(7):1591–602.
[23] Shahzamanian MM, Sahari BB, Bayat M, Ismarrubie ZN, Mustapha F. Transient and thermal contact analysis for the elastic behavior of functionally graded brake disks due to mechanical and thermal loads. Mater Des 2010;31(10):4655–65.
[24] Shahzamanian MM, Sahari BB, Bayat M, Mustapha F, Ismarrubie ZN. Elastic contact analysis of functionally graded brake disks subjected to thermal and mechanical loads. Int J Comput Methods Eng Sci Mech 2013;14(1):10–23.
[25] Ke L-L, Wang Y-S. Two-dimensional sliding frictional contact of functionally graded materials. Eur J Mech-A/Solids 2007;26(1):171–88.
[26] Gunes R, Aydin M, Apalak K, Kemal M, Reddy JN, J. n.,. The elasto-plastic impact analysis of functionally graded circular plates under low-velocities. Compos Struct 2011;93(2):860–9.
[27] Gunes R, Aydin M, Apalak K, Kemal M, Reddy JN, J. n.,. Experimental and numerical investigations of low velocity impact on functionally graded circular plates. Compos B Eng 2014;59:21–32.
[28] Lima DD, Mantri SA, Mikler CV, Contieri R, Yannetta CJ, Campo KN, et al. Laser additive processing of a functionally graded internal fracture fixation plate. Mater Des 2017;130:8–15.
[29] Malekani J. Biomaterials in orthopedic bone plates: a review. Global Science and Technology Forum. 2011.
[30] Lopes ESN, Contieri RJ, Button ST, Caram R. Femoral hip stem prosthesis made of graded elastic modulus metastable β Ti Alloy. Mater Des 2015;69:30–6.
[31] Yang Y, et al. Mg bone implant: Features, developments and perspectives. Mater Des 2020;185:108259.
[32] Krishna KR, Sridhar I, Ghista DN. Analysis of the helical plate for bone fracture fixation. Injury 2008;39(12):1421–36.
[33] Hanada S, Masahashi N, Jung T-K, Yamada N, Yamako Go, Itoi E. Fabrication of a high-performance hip prosthetic stem using β Ti–33.6 Nb–4Sn. J Mech Behav Biomed Mater 2014;30:140–9.
[34] Oladapo BI, et al. Impact of rGO-coated PEEK and lattice on bone implant. Colloids Surf B Biointerfaces 2022;216:112583.
[35] Chandra G, Pandey A, Tipan N. Longitudinally centered embossed structure in the locking compression plate for biodegradable bone implant plate: a finite element analysis. Comput Methods Biomech Biomed Eng 2022;25(6):603–18.
[36] Singh G, Pandey A, Chandra G. Effectiveness of non-uniform thickness on a locking compression plate used as a biodegradable bone implant plate. J Biomater Appl 2022;37(3):429–46.
[37] Fice J, Chandrashekar N. Tapered fracture fixation plate reduces bone stress shielding: a computational study. J Mech Med Biol 2012;12(04):1250072.
[38] Shahzamanian M, Partovi A, Wu P. Finite element analysis of elastic–plastic and fracture behavior in functionally graded materials (FGMs). SN Appl Sci 2020;2(12): 1–11.